

Kent Academic Repository

Full text document (pdf)

Citation for published version

Hall Barrientos, Ivan J. and Paladino, Eleonora and Brozio, Sarah and Passarelli, Melissa K. and Moug, Susan and Black, Richard A. and Wilson, Clive G. and Lamprou, Dimitrios A. (2016) Fabrication and characterisation of drug-loaded electrospun polymeric nanofibers for controlled release in hernia repair. *International Journal of Pharmaceutics*, 517 (1-2). pp. 329-337. ISSN

DOI

<https://doi.org/10.1016/j.ijpharm.2016.12.022>

Link to record in KAR

<http://kar.kent.ac.uk/59857/>

Document Version

Author's Accepted Manuscript

Copyright & reuse

Content in the Kent Academic Repository is made available for research purposes. Unless otherwise stated all content is protected by copyright and in the absence of an open licence (eg Creative Commons), permissions for further reuse of content should be sought from the publisher, author or other copyright holder.

Versions of research

The version in the Kent Academic Repository may differ from the final published version.

Users are advised to check <http://kar.kent.ac.uk> for the status of the paper. **Users should always cite the published version of record.**

Enquiries

For any further enquiries regarding the licence status of this document, please contact:

researchsupport@kent.ac.uk

If you believe this document infringes copyright then please contact the KAR admin team with the take-down information provided at <http://kar.kent.ac.uk/contact.html>

1 **Fabrication and characterisation of drug-loaded electrospun polymeric**
2 **nanofibers for controlled release in hernia repair**

3 **Ivan J. Hall Barrientos^{1,2}, Eleonora Paladino^{2,3,4}, Sarah Brozio², Melissa K. Passarelli⁴,**
4 **Susan Moug⁵, Richard A. Black¹, Clive G. Wilson², Dimitrios A. Lamprou^{2,6*}**

5 ¹ Biomedical Engineering, University of Strathclyde, Glasgow, United Kingdom

6 ²Strathclyde Institute of Pharmacy and Biomedical Sciences (SIPBS), University of
7 Strathclyde, 161 Cathedral Street, Glasgow, G4 0RE, United Kingdom

8 ³EPSRC Centre for Innovative Manufacturing in Continuous Manufacturing and
9 Crystallisation (CMAC), University of Strathclyde, Technology and Innovation Centre, 99
10 George Street, G1 1RD Glasgow, United Kingdom

11 ⁴National Physical Laboratory (NPL), Hampton Road, Teddington, Middlesex, TW11 0LW,
12 United Kingdom

13 ⁵National Health Service (NHS), Royal Alexandra Hospital, Paisley, PA2 9PN, United
14 Kingdom

15 ⁶Medway School of Pharmacy, University of Kent, Medway Campus, Anson Building,
16 Central Avenue, Chatham Maritime, Chatham, Kent, ME4 4TB, United Kingdom

17 * Corresponding author. E-mail address: d.lamprou@kent.ac.uk, Tel.: +441415484968

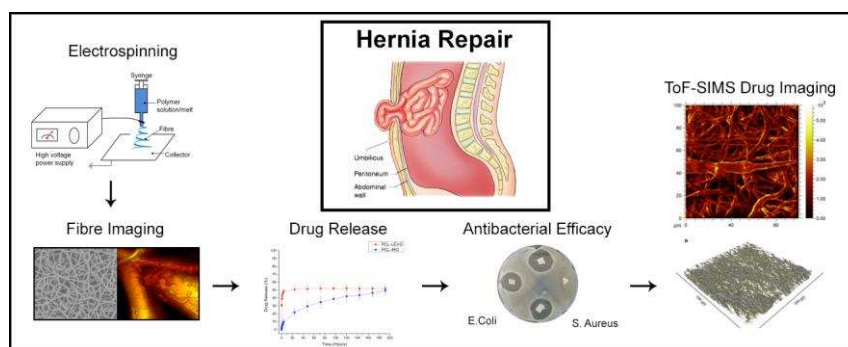
18

19

20 **Abstract**

21 The chemical distribution and mechanical effects of drug compounds in loaded electrospun
 22 scaffolds, a potential material for hernia repair mesh, were characterised and the efficacy of
 23 the material was evaluated. Polycaprolactone electrospun fibres were loaded with either the
 24 antibacterial agent, irgasan, or the broad-spectrum antibiotic, levofloxacin. The samples were
 25 subsequently characterised by rheological studies, scanning electron microscopy (SEM),
 26 atomic force microscopy (AFM), contact angle goniometry (CAG), in vitro drug release
 27 studies, antibacterial studies and time-of-flight secondary ion mass spectrometry (ToF-
 28 SIMS). Increased linear viscoelastic regions observed in the rheometry studies suggest that
 29 both irgasan and levofloxacin alter the internal structure of the native polymeric matrix. In
 30 vitro drug release studies from the loaded polymeric matrix showed significant differences in
 31 release rates for the two drug compounds under investigation. Irgasan showed sustained
 32 release, most likely driven by molecular diffusion through the scaffold. Conversely,
 33 levofloxacin exhibited a burst release profile indicative of phase separation at the edge of the
 34 fibres. Two scaffold types successfully inhibited bacterial growth when tested with strains of
 35 E. coli and S. aureus. Electrospinning drug-loaded polyester fibres is an alternative, feasible
 36 and effective method for fabricating non-woven fibrous meshes for controlled release in
 37 hernia repair.

38



39 **Keywords:** Electrospinning, Scaffolds, Hernia, Drug Release, Physicochemical
40 Characterisation.

41

42

43 **1. Introduction**

44 Hernia repair, one of the most common general surgeries performed, is complicated by
45 bacterial infections and implant rejection [1]. Commercially available mesh devices currently
46 employed in hernia repairs contain braided or knitted fibres. The mechanical properties of the
47 mesh and the biocompatibility of the material are critical to the healing process. Tissue
48 incorporation, a key factor in the success of the graft device is dependent on the material
49 type, density, compliance and electrical properties of the mesh [2]. Graft failure motivates
50 research into new fabrication methods for incorporating biomaterials and drug encapsulation
51 in novel mesh matrices, such as hot-melt extrusion [3], electrospinning [4], 3D printing [5]
52 and high-speed rotary spinning [6].

53 Electrospinning is the most popular and preferred technique for nanofiber fabrication due to
54 its simplicity, cost-effectiveness, flexibility, and ability to spin a broad range of polymers [7].
55 The method allows for the simple and direct functionalization of fibres with drug compounds
56 and is compatible with solvents such as chloroform and dimethyl sulfoxide. In addition, the
57 process of electrospinning with the use of solvents such as chloroform, dimethyl sulfoxide
58 etc., allows functionalisation of the scaffolds through the inclusion of drugs in the polymer-
59 solvent solution without the need for a complicated preparation process [8]. Electrospinning
60 has previously been applied to the fabrication of triclosan/cyclodextrin inclusion complexes
61 [9], the construction of scaffolds with perlecan domain IV peptides [10], manufacture of
62 biocatalytic protein membranes [11], and encapsulation of levofloxacin in mesoporous silica
63 nanoparticles [12]. Given the broad applications of electrospinning, there has been previous
64 research specifically focused on the development of electrospun polymeric materials for
65 hernia repair mesh devices. Electrospinning produces scaffolds containing micro-fibres and
66 this is an advantageous feature not observed in braided mesh commercial devices – these
67 microfibers also introduce mechanical anisotropy and provide topographic features to guide

68 cell alignment [13]. However, electrospun fibres typically incorporate the use of organic
69 solvents and for applications such as hernia repair or tissue engineering, the toxicity of
70 organic solvents used could be highly critical – avoiding organic solvents is of utmost
71 importance for applications in medicine and pharmacy [14], [15].

72 The purpose of this study is to examine the physicochemical properties, bacteria response,
73 and drug loading of electrospun scaffolds. The polymer chosen for this study is
74 polycaprolactone (PCL); a biodegradable polyester commonly used in biomedical
75 applications for controlled release and targeted drug delivery [16]. PCL, a biodegradable
76 aliphatic polyester [17], is an obvious candidate for drug delivery systems due to its high
77 biocompatibility and ease of degradation in the human body [18]. Drug loading of structures
78 that mechanically resemble interfacial tissue and which allows short or long-term release of
79 suitable bioactives may be utilisable in hernia-repair meshes. PCL was chosen in this research
80 as it has a high permeability to a variety of drug molecules (e.g. gentamycin, chitosan) and
81 low toxicity [19]. The matrix was loaded and electrospun with two drugs, irgasan (an
82 antibacterial agent used commonly in soaps, detergents and surgical cleaning agents) or
83 levofloxacin (a broad-spectrum antibiotic used commonly to treat gastrointestinal infections).
84 The mechanical characteristics, morphology, surface hydrophobicity, drug efficacy and
85 chemical distribution were characterised with an array of analytical techniques. The results
86 from this study should help to build platform to aid future work with various fabrication
87 methods, such as extrusion and shaping using 3D printing.

88 **2. Materials & Methods**

89 **2.1 Materials**

90 Polycaprolactone (PCL) with a mean molecular weight of 80 kD, Irgasan (variation of
91 Triclosan, >97%), Levofloxacin (>98%), and all the solvents used for the electrospinning

92 were obtained from Sigma Aldrich. The solvents consisting of chloroform (anhydrous,
93 containing amylenes as stabilizers, >99%) and N,N-dimethylformamide (DMF, anhydrous
94 99.8%).

95 2.2 Preparation of PCL Solutions

96 Different solutions with a polymer concentration of 12% (w/w) were prepared to be used
97 within the electrospinning method – this particular concentration was used due to its
98 possessed suture retention and tensile strengths appropriate for hernia repair, as specified for
99 similar electrospun scaffolds described by Ebersole et al [20]. Various PCL formulations
100 were constructed of a total weight of 25 g per solution, which allowed for PCL (12% w/w)
101 and a 9:1 (w/w) ratio of chloroform (CLF) to N,N-dimethylformamide (DMF). For the
102 unloaded polymer solution, 3 g of PCL was dissolved in 22 g of CLF:DMF (9:1) which was
103 initially mixed through 30 min in a centrifuge, a further 30 min in a sonicator (Elma S30
104 Elmasonic) and a final 1 h with a magnetic stirrer. This process was vital to ensure that the
105 solution was fully homogeneous. The solution was left overnight, and a further 30 min of
106 sonication applied the following morning in order to confirm the homogeneity of the solution.
107 For the irgasan-loaded solutions, the same method was applied, except the solution contained
108 1% (w/w) irgasan. The concentration of the levofloxacin-loaded solutions was 0.5% (w/w),
109 providing sufficient sensitivity in the release cell for accurate UV analysis. All the
110 preparations turned to clear solutions. These observations were interpreted to determine that
111 the solutions had successfully homogenised. The solutions were then subsequently used in
112 the electrospinning process and for rheological analysis.

113 2.3 Electrospinning of PCL Solutions

114 The PCL test specimens were fabricated for each polymeric solution, using a custom in-house
115 electrospinning apparatus, which consisted of a syringe pump (Harvard Apparatus PHD 2000

116 infusion, US) and two 30kV high-voltage power supplies (Alpha III series, Brandenburg,
117 UK). The polymer solution was loaded into glass syringe and fed through tubing with a metal
118 needle tip attached at the end. The needle was clamped into place, to allow a high-voltage
119 supply to run through it, which allowed an electric field to be created between the needle and
120 the target plate. The syringe was clamped to a pump, which determined the specific injection
121 flow rate of the polymeric solutions. For each of the three solutions (e.g. unloaded, irgasan-
122 loaded, and levofloxacin-loaded), 3 varying flow rates of 0.5, 1 and 1.5 ml h⁻¹ were applied
123 across varying voltages of 2 kV – 5 kV (needle) and 10 kV – 18 kV (target plate). The
124 variation in flow rate and applied voltages was to correct any problems that occurred during
125 fabrication, i.e. ‘spitting’ of solution at the target plate, or any potential beading (which was
126 examined through SEM). The fabrication of this solution was electrospun onto the target that
127 was covered with aluminium foil, in order for the final material to be removed and used for
128 further characterisation. The final yield of electrospun PCL resulted in thin, flexible sheets of
129 material.

130 2.4 Rheological Studies

131 A Thermo Scientific HAAKE MARS II rheometer with a P35 TiL cone and plate was used to
132 measure the rheological and mechanical behaviour of the different unloaded and loaded
133 polymeric solutions. The objective of this experiment was to examine the viscoelastic
134 properties of the PCL solution, specifically to determine whether the irgasan or levofloxacin
135 is having an effect on the mechanical properties of the polymer. The method used was taken
136 and modified from the rheological study undertaken by Bubel et al [15]. In briefly, an
137 oscillating amplitude sweep between 0.1 Pa – 1000 Pa at a frequency of 1 Hz was used to
138 determine the linear viscoelastic region (LVER) of the samples. Once the LVER is
139 determined from the amplitude sweep, a downwards oscillating frequency sweep from 10 Hz
140 – 0.1 Hz with a shear stress (Pa) within the LVER was then used in order to help understand

141 the nature of the solutions concerning strength and stability. The experiments were repeated 4
142 times per solution, and for each experiment, each data point (20 data points per method) was
143 optimised to repeat each measurement 5 times.

144 2.5 Scanning Electron Microscopy (SEM)

145 The morphology and diameter of individual fibres spun from PCL solution were determined
146 from scanning electron micrographs of each sample (TM-1000, Hitachi, UK, Ltd.). The
147 samples were mounted on an aluminium plate with conductive tape. Images of fibres were
148 taken at various locations of each electrospun PCL scaffold in order to determine the overall
149 uniformity of fibres. Prior to imaging, the samples were sputter coated with gold for 30 sec
150 using a Leica EM ACE200 vacuum coater, the process being repeated four times in order to
151 increase the conductivity of the samples.

152 2.6 Atomic Force Microscopy (AFM)

153 Further morphological analysis was undertaken through atomic force microscopy. A
154 Multimode 8 microscope (Bruker, USA), with Scanasyst-Air probes (Bruker, USA) was used
155 in Peak Force Quantitative Nano Mechanics (QNM) mode, as described by Lamprou et al
156 [21]. The imaging of the fibres was performed under ambient conditions, with a silicon
157 cantilever probe. The tip radius of the probe and the spring constant were calculated to be in
158 the regions of 0.964 nm (18° tip half angle) and 0.4935 N/m, respectively. The scan sizes
159 ranged from 200 nm to 25 µm, at a scan rate of 0.977 Hz with 256-sample resolution. The
160 Roughness Average (Ra) values were determined by entering surface scanning data, and
161 digital levelling algorithm values were determined using Nanoscope Analysis software V1.40
162 (Bruker USA). AFM images were collected from two different samples and at random spot
163 surface sampling.

164 2.7 Contact Angle Goniometry (CAG)

165 To monitor changes in wettability of the scaffolds, sessile drop contact angle for distilled
166 water was measured by contact angle goniometry, using a contact angle goniometer (Kruss
167 G30, Germany) as described by Lamprou et al [22].

168 2.8 In Vitro Drug Release Studies

169 The drug releases of the irgasan/levofloxacin loaded PCL scaffolds were measured in order to
170 determine the release profile of the drugs. Samples of PCL-IRG were immersed in phosphate
171 buffered saline (PBS) containing 0.5% sodium dodecyl sulfate (SDS) at 37 °C, and samples
172 of PCL-LEVO were immersed in PBS only at 37 °C. This release study was based on the
173 method cited by Duan et al [23]. The solutions were agitated using a shaker at a rate of 80
174 rev/min. The UV absorbance of both drugs was measured: irgasan at 280 nm [24], and
175 levofloxacin at 292 nm [25] respectively. Measurements were taken at intervals at 15 min, 30
176 min, 1 h, 2 h, 4 h, 8 h, 24 hrs and every day after the 24 h mark for up to 7 days. At each
177 point, 4 ml of solution was taken from the vial and replaced with fresh in order to satisfy the
178 perfect-sink conditions and keeping the volume of the solution constant.

179 2.9 Antibacterial Studies

180 The antibacterial efficacy of the drug loaded electrospun scaffolds were tested against
181 *Escherichia coli* (*E. coli*) 8739 and *Staphylococcus aureus* (*S. aureus*) 29213. *S. aureus* is
182 Gram positive, *E. coli* is Gram negative and both bacteria are common causes of nosocomial
183 infections. . Both irgasan and levofloxacin should have antibacterial effects. For this study, an
184 agar diffusion method was used. Luria-Bertani (LB) agar was prepared from a formulation of
185 5 g tryptone, 2.5 g yeast extract, 5 g NaCl in 475 ml of deionized water. The LB agar was
186 autoclaved and poured into 20ml plates. The *E. coli* and *S. aureus* were grown overnight in 5

187 ml of LB Broth, with both bacteria inoculated from a single colony. 150 μ L of the *E. coli* and
188 *S. aureus* cultures were spread onto six different plates of LB agar. Three plates consisted of
189 spread *E. coli*, including a scaffold free plate, which acted as a control – the other 2 plates,
190 were divided into 4 sections, with 1 section containing an unloaded PCL scaffold, and the
191 other 3 containing PCL-irgasan and PCL-levofloxacin scaffolds. This procedure was repeated
192 for three plates of spread *S. aureus*. The plates were incubated for 24 h, and subsequently
193 examined. Diameters of the zones of growth inhibition were measured, and these data
194 compared across the drugs and bacterial strains. This method was based on the method
195 described by Davachi et al [26].

196 2.10 Time of Flight Secondary Ion Mass Spectrometry (ToF-SIMS)

197 ToF-SIMS data was acquired using a ToF-SIMS V mass spectrometer (ION-TOF GmbH,
198 Münster, Germany) based at the Wolfson Foundation Pharmaceutical Surfaces Laboratory at
199 the University of Strathclyde. The instrument is equipped with a bismuth liquid metal ion
200 gun (LMIG), an argon gas cluster ion beam (GCIB) and a gridless reflectron time-of-flight
201 mass analyzer.

202 Three different acquisition modes, detailed below, were used to analyse the fibres: high mass
203 resolution spectroscopy, depth profiling, high lateral resolution imaging. Owing to the
204 insulative nature of the materials, a low-energy electron beam (21 V) was used to compensate
205 for charging.

206 2.10.1 High Mass Resolution Spectroscopy

207 For an optimal mass resolution, the primary ion beam (Bi_3^{++} primary ions) was pulsed at 10
208 kHz frequency with a pulse width of 17.0 ns. The primary ion gun energy was set at 30 kV
209 and the pulsed target current was approximately 0.63 pA. Data was collected both in the

210 positive and in the negative secondary ion polarities, in three replicates; each acquisition was
211 made from different areas of the samples used in this study. The analysed area and the
212 acquisition time, for each repetition, were respectively $100\ \mu\text{m} \times 100\ \mu\text{m}$ and 120 seconds,
213 delivering a primary ion dose density (PIDD) of approximately 4.6×10^{12} (primary ions/cm²).
214 Reference spectra for pure Levofloxacin and Irgasan compounds were acquired in positive
215 and negative ion mode from 0 to 400 Da.

216 2.10.2 High Lateral Resolution Imaging

217 The LMIG was operated using the imaging mode, with high lateral resolution, and Bi₃⁺⁺ was
218 selected as primary ion beam. The primary ion gun energy was 30 kV and the pulsed target
219 current was approximately 0.048 pA. High lateral resolution ion images were collected over a
220 surface area of $100\ \mu\text{m} \times 100\ \mu\text{m}$, using a pulsed analysis beam (pulse width = 100 ns). The
221 resolution was 256×256 pixels per image (pixel width was circa 0.4 μm). Each image was
222 obtained with a final ion dose of 6.5×10^{12} primary ions/cm² or less. The dose was kept
223 below the static limit of 10^{13} primary ions/cm² to minimize surface damages during the
224 analysis. The images were processed with the ION-TOF SurfaceLab 6.6 software (Münster,
225 Germany).

226 2.10.3 3D Imaging

227 The LMIG and the GCIB were employed in a dual-beam configuration to collect the depth
228 profile and the 3D image data. The LMIG was operated in pulsed mode to investigate the
229 lateral distribution of chemical species, while the Argon source was operated in DC mode to
230 remove multiple layers of material from the sample surface between the analytical cycles. For
231 the depth profiling analysis, the dual beam experiment used a 30 kV Bi₃⁺⁺ primary ion beam
232 for analysis and a 10 kV Ar₁₅₀₀⁺ beam for sputtering. The pulsed current of the Bi₃⁺⁺ primary
233 ion beam was 0.048 pA and the DC current of the cluster Ar₁₅₀₀⁺ was 10.22 nA, with a 500

234 seconds analysis time and 4 seconds sputtering time. The raster areas of the pulsed analysis
235 beams and the DC sputter were $100\ \mu\text{m} \times 100\ \mu\text{m}$ and $300\ \mu\text{m} \times 300\ \mu\text{m}$, respectively. The
236 resolution was 256×256 pixels per image (pixel width of about $0,4\ \mu\text{m}$). Data was collected
237 in the negative secondary ion mode. In the course of each acquisition, mass spectral
238 information at each image pixel was collected in the m/z range of 0-917 m/z .

239 2.11 Statistical Analysis

240 All experiments were performed in triplicate with calculation of means and standard
241 deviations. Two-way analysis of variance (ANOVA) was used for multiple comparisons
242 along with Tukey's multiple comparing tests, followed by T-test to assess statistical
243 significance for paired comparisons. Significance was acknowledged for p values lower than
244 0.05.

245 3. Results and discussion

246 3.1 Rheological Studies

247 For each polymeric solution, multiple amplitude sweeps were used in order to correctly
248 identify the linear viscoelastic region (LVR). This was repeated to detect any major variations
249 in the LVR, and for a more accurate shear stress to be used in the frequency sweeps. For each
250 of the samples, elastic modulus (G'), viscous modulus (G'') and shear viscosity (η) was
251 calculated and subsequently analysed.

252 It can be seen in figure 1 that for all three solutions, the viscosity modulus (from 30 Pa to 80
253 Pa) is considerably greater than the elastic modulus (0.5 Pa to 6 Pa) which implies that the
254 solutions exhibit significantly less elastic properties. As observed in figure 1c, both polymer-
255 drug-loaded solutions of irgasan and levofloxacin show differences in the shear viscosity (η).
256 The amplitude sweep demonstrated that these drugs caused a reduction in all three of these

257 parameters – this may be caused by the possible transition from semi-dilute to dilute regime,
258 where there are less polymer chain entanglements [27]. It is also worth noting that the LVR
259 for the drug-loaded solutions was extended; the unloaded PCL solution had a short LVR of
260 between 50 Pa to 100 Pa (shear stress), which then resulted in shear thinning at high shear
261 stresses. These long LVRs are indicative of well-dispersed, stable polymer-drug systems.
262 This behaviour of Newtonian to shear thinning has been previously observed in other studies;
263 it can be attributed to the formation of physical bonding between the drug and the polymer,
264 which causes an increase in the solution viscosity [28].

265 The frequency sweep data shown in figure 2 are indicative of how the drug dispersed in the
266 matrix affected the overall structure. Again, it was observed that loading the polymer solution
267 with drugs had an effect, with measured viscosity in all three samples appearing to be
268 frequency dependent. According to data in both G' and G'' graphs, G'' was shown to be the
269 dominating effect (G' ranging from seven to 30 Pa, and G'' ranging from 150 to 175 Pa).
270 Long regions of viscoelasticity normally imply that there is a certain degree of stability
271 within the polymer matrix; however, the frequency sweep implies otherwise. It appears that
272 G' and G'' are both frequency dependent, which implies that the system has little internal
273 network and is easily disturbed [15].

274 3.2 Fibre Morphology

275 Figure 3 shows SEM images of the various unloaded and drug-loaded PCL scaffolds. Smooth
276 morphology can be observed in all 3 different scaffolds and at a 12% concentration of
277 polymer, there is no significant beading or any visible signs of either API outside of the
278 fibres. The major differences across the three different scaffolds are the fibre size – the
279 addition of irgasan reduced the average fibre diameter to $1.623 \pm 1.9 \mu\text{m}$. These fibres appear
280 to be relatively consistent in size compared to other various PCL-fibre studies, $1.1 \pm 6.6 \mu\text{m}$,

281 $2.7 \pm 2.0 \mu\text{m}$ and $1.83 \pm 0.050 \mu\text{m}$ [9], [29], [30]. The morphology of the levofloxacin-loaded
282 fibres appeared to differ from the unloaded and irgasan loaded fibres: whilst there appears to
283 be a smooth morphology, the fibres appear more densely packed with a greater ‘curvature’ of
284 the fibres. These fibres are also greater in diameter in comparison with the PCL-IRG scaffold,
285 with an average fibre diameter of $2.865 \pm 3.0 \mu\text{m}$. The PCL-LEVO fibres appear to be much
286 larger in diameter compared with studies by Jalvandi et al [12] (600 – 800 nm), Puppi et al
287 [31] ($219.2 \pm 55.1 \text{ nm}$) and Park et al [32] ($232 \pm 20.4 \text{ nm}$). This variation in fibre diameter
288 could possibly be attributed to the higher voltage applied to the target plate during the
289 electrospinning process – for PCL and PCL-IRG solutions, the voltage applied varied
290 between 10 – 12 kV whereas the PCL-LEVO solution was $\pm 18 \text{ kV}$. There is a critical value
291 of applied voltage, and the increase in the diameter with an increase in the applied voltage are
292 attributed to the decrease in the size of the Taylor cone and increase in the jet velocity for the
293 same flow rate [33].

294 Considering the morphology of the fibres at a greater detail and image resolution, the AFM
295 characterisation showed a significant difference between the irgasan-loaded and levofloxacin-
296 loaded fibres. Figure 4a shows the smooth morphology of the PCL-IRG scaffold at a 400 nm
297 scale, and it can be clearly seen that there appears to be no signs of API on the surface of the
298 polymer. This suggests that the irgasan is integrated into the polymeric matrix. In contrast, it
299 was found using AFM that within certain areas of the PCL-LEVO scaffold, there appeared to
300 be regions with crystalline API sitting at the surface (figure 4b).

301 3.3 Surface Characterisation

302 The CAG results for the irgasan-loaded fibres indicated an increase in the hydrophobicity of
303 the scaffold in comparison to the unloaded PCL scaffold – the water drop took 45 minutes to
304 absorb fully into the PCL-IRG scaffold, and this slow nature of absorption potentially

305 indicates that the irgasan may release in a sustained mechanism. This is most likely due to the
306 hydrophobic nature of irgasan combined within the polymeric matrix of PCL, which also has
307 a certain degree of hydrophobicity. The CAG results for the levofloxacin-loaded scaffolds
308 were inconclusive given that hydrophilic nature of levofloxacin- the water droplet applied
309 was absorbed almost immediately; therefore, no data could be obtained. However, this does
310 support the hypothesis that there may be an amount of levofloxacin sitting at the surface of
311 the sample – the quick absorbance of the water droplet may be the levofloxacin uptake.

312 3.4 Drug Efficacy of Electrospun Scaffolds

313 The release of irgasan (figure 5) from the PCL-irgasan scaffold appeared to exhibit sustained
314 release behaviour of the encapsulated drug. The final cumulative drug release was found to
315 be at 50 %; although more irgasan will be released beyond 200 h (equilibrium had not been
316 observed at the 200 hr). The behaviour of the PCL-levofloxacin scaffold was entirely
317 different to the irgasan-loaded scaffold. It exhibited burst release behaviour and the antibiotic
318 was almost entirely lost from the matrix within the first 15 min of measurements.. The final
319 cumulative drug release was also found to be at 50 %. This burst release behaviour is
320 consistent with the manner in which the drug is associated with the polymer matrix – the
321 previous SEM and AFM were indicative of the presence of levofloxacin on the surface of the
322 fibres in some areas.

323 Determining the drug release profiles of the drugs was a crucial part of this study, as
324 divergent behaviours helped us to characterise bridging properties indicating the manner in
325 which irgasan and levofloxacin dispersed within the polymer matrix. The irgasan released
326 steadily over 145 hours, which would suggest that the drug is being released through
327 molecular diffusion [34]. The levofloxacin exhibited a burst release mechanism, although this

328 may be attributed to the mechanism in which levofloxacin functions in most polymers [32],
329 due to the way the drug is adsorbed on to the surface of the polymer [31], [35].

330 The main factors that could be expected to influence the drug release kinetics in this study
331 can be summarised as follows are:

- 332 • Material matrix: this includes the composition, structure and degradation of polymer;
333 however, the polymer showed no signs of degradation and is known to show a high
334 degree of stability.
- 335 • Release medium: the irgasan was released in a buffer of PBS and sodium dodecyl
336 sulphate (surfactant), therefore it could be suggested either that the surfactant is
337 interacting with the polymer/drug or that it is changing the ionic strength of the buffer
338 [36].
- 339 • Drug compounds: Fu and Kao [34] cite solubility, stability charges and interaction
340 with matrix as major factors with the drug that may affect the drug release kinetics.
341 The results in our studies can demonstrate this, given that potential charges of the
342 drug were affecting fabrication, therefore it can be assumed that the charges of irgasan
343 and levofloxacin may be affecting the drug release kinetics.

344 3.5 In-Vitro Antibacterial Activity

345 The antibacterial efficacy (Figure 6) of both irgasan and levofloxacin-loaded scaffolds were
346 tested against strains of *E. coli* and *S. aureus*, with the efficacy specifically determined by
347 visual zones of inhibition on the agar plate. The PCL-irgasan scaffold showed signs of some
348 activity, albeit weak, against *E. coli* with an average inhibition zone diameter of 0.7 ± 0.5 cm.
349 However, the irgasan-loaded scaffold was particularly successful inhibiting the growth of *S.*
350 *aureus* with an average inhibition zone diameter of 1.8 ± 0.5 cm. There was a higher-level
351 efficacy observed within the PCL-levofloxacin cultures of both *E. coli* and *S. aureus*. Both

352 strains of bacteria were inhibited on the agar plate with an average diameter of no growth of
353 2.6 cm. The antibacterial studies have shown that there is a high efficacy of bacteria
354 inhibition in both irligan and levofloxacin-loaded scaffolds across *E. coli* and *S. aureus*
355 bacteria. The levofloxacin-loaded scaffolds demonstrated larger values of inhibition zones,
356 for both bacteria – this should be the case, given that levofloxacin is a broad-spectrum
357 antibiotic, active against both gram positive and gram negative. The irligan-loaded scaffold
358 showed stronger inhibition to the *S. aureus* bacteria; however, this should not be viewed as a
359 negative result. *S. aureus* is a gram-positive bacterium that is commonly found on the skin,
360 therefore is a major cause of nosocomial wound infection [37]. The hydrophobic natures of
361 irligan and PCL, and potential stronger interactions between drug and polymer are likely to
362 aid the sustained release from the fibres – this sustained release can be observed in the
363 previous in vitro drug release study, and observed in the reduced inhibition of *E. Coli* [9].

364 3.6 ToF-SIMS Analysis

365 Imaging and 3D imaging techniques showed a difference in the distribution of the active
366 pharmaceutical ingredients (API) between Irganon-loaded and Levofloxacin-loaded fibres.
367 PCL is identified by the ion at m/z 113 ($[C_6H_9O_2]^- [M-H]^-$), Levofloxacin by the ions at m/z
368 360 ($[C_{18}H_{19}FN_3O_4]^- [M-H]^-$) and m/z 316 ($[C_{17}H_{19}FN_3O_2]^-$), and Irganon by the ions at m/z
369 287 ($[C_{12}H_6^{35}Cl_3O_2]^- [M-H]^-$), m/z 289 ($[C_{12}H_6^{35}Cl_2^{37}Cl_1O_2]^-$) and m/z 291
370 ($[C_{12}H_6^{35}Cl_1^{37}Cl_2O_2]^-$). The total ion images and the overlays of single ion images for the
371 characteristic peaks of PCL (grey) and the two drugs (yellow) are reported in Figure 7. The
372 ion images show a homogeneous distribution of Irganon, throughout the electrospun fibres,
373 whilst the Levofloxacin appears to be concentrated in several small areas. This was
374 confirmed by 3D imaging, where Irganon characteristic peaks appeared to be homogeneously
375 distributed in the volume (Figure 8a). Conversely, Levofloxacin had an intense signal
376 localized to small areas and mainly on the surface (Figure 8b).

377 **4. Conclusions**

378 The purpose of this study was to fabricate drug-loaded fibres that may potentially be used
379 within a hernia repair context. The good understanding of the relationship between the
380 solution viscosity and the spinning parameters is essential if the technique is to be effective,
381 hence the need to characterise the effect of drug loading on the rheological behaviour of the
382 spinning solutions. It was observed that the addition of both irgasan and levofloxacin had a
383 direct influence on the rheological behaviour of the solutions; a reduction in elastic modulus,
384 viscous modulus, and shear viscosity occurred, which may cause a reduction in polymer
385 chain entanglements. However, this explanation may not be the only viable one – rheological
386 behaviour of drug-loaded solutions has been widely researched, although further
387 characterisation into the molecular interactions between drug and polymer may give further
388 insight into why the solution behaviour changes significantly. Atomic force microscopy
389 indicated that crystals, probably of levofloxacin were present on the surface of the polymer
390 fibres, and this was crucial in explaining the behaviour of the drug during in vivo release
391 studies and antibacterial activity profile. The presence of levofloxacin at the surface of the
392 polymer was confirmed through contact angle goniometry (immediate absorbance of the
393 water droplet showed the hydrophilic nature of levofloxacin in action), in vitro release studies
394 (the drug demonstrated a burst release behaviour), antibacterial studies (an increased average
395 inhibition zone repelled both bacteria types immediately) and ToF-SIMS. In the ToF-SIMS
396 study, the molecular weight of levofloxacin was shown at various areas across the fibres and
397 the 3D imaging of the matrix indicated there was a certain degree of drug encapsulation. This
398 study has contrasted the incorporation of two different drugs within an electrospun fibre, and
399 shown that through bridging chemical, mechanical and biological studies, their behaviours
400 can be fully interpreted. The next stages of this research are to now assess whether these

401 constructs are useful within any clinical scenario, and in particular, within the treatment of
402 hernia repair.

403 **Acknowledgements**

404 The authors would like to thank the UK Engineering & Physical Sciences Research Council
405 (EPSRC) Doctoral Training Centre in Medical Devices, University of Strathclyde (EPSRC
406 Grant Ref. EP/F50036X/1) for the studentship awarded to IHB. The authors would also like
407 to thank the EPSRC Centre in Continuous Manufacturing and Crystallisation (CMAC) for
408 access to specialised instruments.

409

410 **References**

- 411 [1] D. B. Earle, “Biomaterials in Hernia Repair,” 2010. [Online]. Available:
412 [http://laparoscopy.blogs.com/prevention_management_3/2010/08/biomaterials-in-](http://laparoscopy.blogs.com/prevention_management_3/2010/08/biomaterials-in-hernia-repair.html)
413 [hernia-repair.html](http://laparoscopy.blogs.com/prevention_management_3/2010/08/biomaterials-in-hernia-repair.html). [Accessed: 15-Sep-2015].
- 414 [2] L. Procter, E. E. Falco, J. P. Fisher, and J. S. Roth, “Abdominal Wall Hernias &
415 Biomaterials,” in *Bioengineering Research of Chronic Wounds*, 1st ed., A. Gefen, Ed.
416 Berlin: Springer Verlag, 2009, pp. 425–447.
- 417 [3] D. Li, G. Guo, R. Fan, J. Liang, X. Deng, F. Luo, and Z. Qian,
418 “PLA/F68/Dexamethasone implants prepared by hot-melt extrusion for controlled
419 release of anti-inflammatory drug to implantable medical devices: I. Preparation,
420 characterization and hydrolytic degradation study,” *Int. J. Pharm.*, vol. 441, no. 1–2,
421 pp. 365–372, 2013.
- 422 [4] A. Toncheva, D. Paneva, N. Manolova, and I. Rashkov, “Electrospun poly(L-lactide)
423 membranes containing a single drug or multiple drug system for antimicrobial wound
424 dressings,” *Macromol. Res.*, vol. 19, no. 12, pp. 1310–1319, 2011.
- 425 [5] J. Holländer, N. Genina, H. Jukarainen, M. Khajeheian, A. Rosling, E. Mäkilä, and N.
426 Sandler, “Three-Dimensional Printed PCL-Based Implantable Prototypes of Medical
427 Devices for Controlled Drug Delivery,” *J. Pharm. Jenny, Natalja Genina, Harri*
428 *Jukarainen, Mohammad Khajeheian, Ari Rosl. Ermei Mäkilä, Niklas Sandler. “Three-*
429 *Dimensional Print. PCL-Based Implant. Prototypes Med. Devices Control. Drug*
430 *Deliv. J*, vol. 105, 2016.
- 431 [6] I. Sebe, B. Szabo, Z. K. Nagy, D. Szabo, L. Zsidai, B. Kocsis, and R. Zelko, “Polymer
432 structure and antimicrobial activity of polyvinylpyrrolidone-based iodine nanofibres

- 433 prepared with high-speed rotary spinning technique,” *Int. J. Pharm.*, vol. 458, no. 1,
434 pp. 99–103, 2013.
- 435 [7] M. Zamani, M. P. Prabhakaran, and S. Ramakrishna, “Advances in drug delivery via
436 electrospun and electrosprayed nanomaterials,” *Int. J. Nanomedicine*, vol. 8, pp. 2997–
437 3017, 2013.
- 438 [8] M. He, J. Xue, H. Geng, H. Gu, D. Chen, R. Shi, and L. Zhang, “Fibrous guided tissue
439 regeneration membrane loaded with anti-inflammatory agent prepared by coaxial
440 electrospinning for the purpose of controlled release,” *Appl. Surf. Sci.*, vol. 335, pp.
441 121–129, 2015.
- 442 [9] A. Celebioglu, O. C. O. Umu, T. Tekinay, and T. Uyar, “Antibacterial electrospun
443 nanofibers from triclosan/cyclodextrin inclusion complexes,” *Colloids Surfaces B
444 Biointerfaces*, vol. 116, pp. 612–619, 2014.
- 445 [10] O. Hartman, C. Zhang, E. L. Adams, M. C. Farach-carson, J. Petrelli, B. D. Chase, and
446 J. F. Rabolt, “Biofunctionalization of electrospun PCL-based scaffolds with perlecan
447 domain IV peptide to create a 3-D pharmacokinetic cancer model,” *Biomaterials*, vol.
448 31, no. 21, pp. 5700–5718, 2011.
- 449 [11] G. Kabay, G. Kaleli, Z. Sultanova, T. T. Ölmez, U. Ö. Ş. Şeker, and M. Mutlu,
450 “Biocatalytic protein membranes fabricated by electrospinning,” *React. Funct. Polym.*,
451 vol. 103, pp. 26–32, 2016.
- 452 [12] J. Jalvandi, M. White, Y. B. Truong, Y. Gao, R. Padhye, and I. L. Kyratzis, “Release
453 and antimicrobial activity of levofloxacin from composite mats of poly(e-
454 caprolactone) and mesoporous silica nanoparticles fabricated by core-shell
455 electrospinning,” *J. Mater. Sci.*, vol. 50, no. 24, pp. 7967–7974, 2015.

- 456 [13] A. S. Goldstein and P. S. Thayer, "Fabrication of complex biomaterial scaffolds for
457 soft tissue engineering by electrospinning," in *Nanobiomaterials in Soft Tissue*
458 *Engineering*, A. Grumezescu, Ed. Amsterdam: William Andrew, 2016, pp. 299–330.
- 459 [14] S. Agarwal and A. Greiner, "On the way to clean and safe electrospinning-green
460 electrospinning: Emulsion and suspension electrospinning," *Polym. Adv. Technol.*, vol.
461 22, no. 3, pp. 372–378, 2011.
- 462 [15] K. Bubel, D. Grunenber, G. Vasilyev, E. Zussman, S. Agarwal, and A. Greiner,
463 "Solvent-Free Aqueous Dispersions of Block Copolyesters for Electrospinning of
464 Biodegradable Nonwoven Mats for Biomedical Applications," *Macromol. Mater.*
465 *Eng.*, pp. 1445–1454, 2014.
- 466 [16] M. D. Bhavsar and M. M. Amiji, "Development of novel biodegradable polymeric
467 nanoparticles-in-microsphere formulation for local plasmid DNA delivery in the
468 gastrointestinal tract.," *AAPS PharmSciTech*, vol. 9, no. 1, pp. 288–94, 2008.
- 469 [17] B. Azimi, P. Nourpanah, M. Rabiee, and S. Arbab, "Poly (lactide -co- glycolide)
470 Fiber : An Overview."
- 471 [18] D. N. Bikiaris, G. Z. Papageorgiou, D. S. Achilias, E. Pavlidou, and A. Stergiou,
472 "Miscibility and enzymatic degradation studies of poly(ϵ -caprolactone)/poly(propylene
473 succinate) blends," *Eur. Polym. J.*, vol. 43, no. 6, pp. 2491–2503, 2007.
- 474 [19] R. S. R. Murthy, "Biodegradable Polymers," N. K. Jain, Ed. New Dehli: CBS
475 Publisher, 1997, pp. 27–51.
- 476 [20] G. C. Ebersole, E. G. Buettmann, M. R. MacEwan, M. E. Tang, M. M. Frisella, B. D.
477 Matthews, and C. R. Deeken, "Development of novel electrospun absorbable
478 polycaprolactone (PCL) scaffolds for hernia repair applications," *Surg. Endosc. Other*

- 479 Interv. Tech., vol. 26, no. 10, pp. 2717–2728, 2012.
- 480 [21] D. A. Lamprou, V. Venkatpurwar, and M. N. V. R. Kumar, “Atomic Force
481 Microscopy Images Label-Free, Drug Encapsulated Nanoparticles In Vivo and Detects
482 Difference in Tissue Mechanical Properties of Treated and Untreated: A Tip for
483 Nanotoxicology,” PLoS One, vol. 8, no. 5, pp. 8–12, 2013.
- 484 [22] D. A. Lamprou, J. R. Smith, T. G. Nevell, E. Barbu, C. R. Willis, and J. Tsibouklis,
485 “Self-assembled structures of alkanethiols on gold-coated cantilever tips and substrates
486 for atomic force microscopy: Molecular organisation and conditions for reproducible
487 deposition,” Appl. Surf. Sci., vol. 256, no. 6, pp. 1961–1968, 2010.
- 488 [23] K. DUAN, D. XIAO, and J. WENG, “Triclosan-loaded PLGA microspheres-porous
489 titanium composite coating,” pp. 1–6, 2013.
- 490 [24] A. Piccoli, J. Fiori, V. Andrisano, and M. Orioli, “Determination of triclosan in
491 personal health care products by liquid chromatography (HPLC),” Farmaco, vol. 57,
492 no. 5, pp. 369–372, 2002.
- 493 [25] M. Maleque, M. R. Hasan, F. Hossen, and S. Safi, “Development and validation of a
494 simple UV spectrophotometric method for the determination of levofloxacin both in
495 bulk and marketed dosage formulations,” J. Pharm. Anal., vol. 2, no. 6, pp. 454–457,
496 2012.
- 497 [26] S. M. Davachi, B. Kaffashi, A. Zamanian, B. Torabinejad, and Z. Ziaeirad,
498 “Investigating composite systems based on poly l-lactide and poly l-lactide/triclosan
499 nanoparticles for tissue engineering and medical applications,” Mater. Sci. Eng. C, vol.
500 58, pp. 294–309, 2016.
- 501 [27] J. R. Dias, F. E. Antunes, and P. J. Bártolo, “Influence of the rheological behaviour in

- 502 electrospun PCL nano fibres production for tissue engineering application,” *Chem.*
503 *Eng. Trans.*, vol. 32, no. 2011, pp. 1015–1020, 2013.
- 504 [28] Z. Sadrearhami, M. Morshed, and J. Varshosaz, “Production and evaluation of
505 polyblend of agar and polyacrylonitrile nanofibers for in vitro release of methotrexate
506 in cancer therapy,” *Fibers Polym.*, vol. 16, no. 2, pp. 254–262, 2015.
- 507 [29] N. Detta, T. D. Brown, F. K. Edin, K. Albrecht, F. Chiellini, E. Chiellini, P. D. Dalton,
508 and D. W. Hutmacher, “Melt electrospinning of polycaprolactone and its blends with
509 poly(ethylene glycol),” *Polym. Int.*, vol. 59, no. 11, pp. 1558–1562, 2010.
- 510 [30] L. J. Del Valle, R. Camps, A. Díaz, L. Franco, A. Rodríguez-Galán, and J. Puiggali,
511 “Electrospinning of polylactide and polycaprolactone mixtures for preparation of
512 materials with tunable drug release properties,” *J. Polym. Res.*, vol. 18, no. 6, pp.
513 1903–1917, 2011.
- 514 [31] D. Puppi, D. Dinucci, C. Bartoli, C. Mota, C. Migone, F. Dini, G. Barsotti, F. Carlucci,
515 and F. Chiellini, “Development of 3D wet-spun polymeric scaffolds loaded with
516 antimicrobial agents for bone engineering,” *J. Bioact. Compat. Polym.*, vol. 26, pp.
517 478–492, 2011.
- 518 [32] H. Park, H. Yoo, T. Hwang, T. J. Park, D. H. Paik, S. W. Choi, and J. H. Kim,
519 “Fabrication of levofloxacin-loaded nanofibrous scaffolds using coaxial
520 electrospinning,” *J. Pharm. Investig.*, vol. 42, no. 2, pp. 89–93, 2012.
- 521 [33] A. Haider, S. Haider, and I. K. Kang, “A comprehensive review summarizing the
522 effect of electrospinning parameters and potential applications of nanofibers in
523 biomedical and biotechnology,” *Arab. J. Chem.*, 2015.
- 524 [34] F. Yao and J. K. Weiyuan, “Drug Release Kinetics and Transport Mechanisms of Non-

- 525 degradable and Degradable Polymeric Delivery Systems,” *Expert Opin. Drug Deliv.*,
526 vol. 7, no. 4, pp. 429–444, 2010.
- 527 [35] W. S. Cheow, M. W. Chang, and K. Hadinoto, “Antibacterial efficacy of inhalable
528 levofloxacin-loaded polymeric nanoparticles against *E. coli* biofilm cells: The effect of
529 antibiotic release profile,” *Pharm. Res.*, vol. 27, no. 8, pp. 1597–1609, 2010.
- 530 [36] M. Thongngam and D. J. McClements, “Influence of pH, ionic strength, and
531 temperature on self-association and interactions of sodium dodecyl sulfate in the
532 absence and presence of chitosan,” *Langmuir*, vol. 21, no. 1, pp. 79–86, 2005.
- 533 [37] M. Sisirak, A. Zvizdic, and M. Hukic, “Methicillin-resistant *Staphylococcus aureus*
534 (MRSA) as a cause of nosocomial wound infections,” *Bosn. J. Basic Med. Sci.*, vol.
535 10, no. 1, pp. 32–37, 2010.
- 536

537 **Figure Captions**

538 **Figure 1 a:** Amplitude sweep viscous modulus (G') data for PCL, PCL-IRG and PCL-LEVO
539 solutions; **b:** Amplitude sweep viscous modulus (G'') data for PCL, PCL-IRG and PCL-
540 LEVO solutions; **c:** Amplitude sweep shear viscosity (η) data for PCL, PCL-IRG and PCL-
541 LEVO solutions.

542 **Figure 2 a:** Frequency sweep elastic modulus (G') data for PCL, PCL-IRG and PCL-LEVO
543 solutions; **b:** Frequency sweep viscous modulus (G'') data for PCL, PCL-IRG and PCL-
544 LEVO solutions; **c:** Frequency sweep shear viscosity (η) data for PCL, PCL-IRG and PCL-
545 LEVO solutions.

546 **Figure 3:** SEM images of PCL (a), PCL-IRG (b) and PCL-LEVO (c) electrospun fibres.

547 **Figure 4 a:** AFM image of PCL-IRG fibres; **b:** AFM image of PCL-LEVO fibres.

548 **Figure 5:** Cumulative drug release percentages for the release of IRG and LEVO in PBS
549 media.

550 **Figure 6:** Images showing the average zone of inhibition of PCL-IRG and PCL-LEVO
551 against bacterial strains of *E. coli* and *S. aureus*.

552 **Figure 7a/b:** The images above are acquired with a high lateral resolution mode, which
553 enables to easily visualise the nanofibers (total ion image A and B) and the distribution of the
554 API (colour overlay images C and D); **c:** Overlay of $[\text{C}_6\text{H}_9\text{O}_2]^-$ (PCL) in grey and
555 $[\text{C}_{12}\text{H}_6\text{Cl}_3\text{O}_2]^-$ (Irgasan) in yellow; **d:** Overlay of $[\text{C}_6\text{H}_9\text{O}_2]^-$ (PCL) in grey and of
556 $[\text{C}_{17}\text{H}_{19}\text{FN}_3\text{O}_2]^-$ and $[\text{C}_{18}\text{H}_{19}\text{FN}_3\text{O}_4]^-$ (Levofloxacin) in yellow.

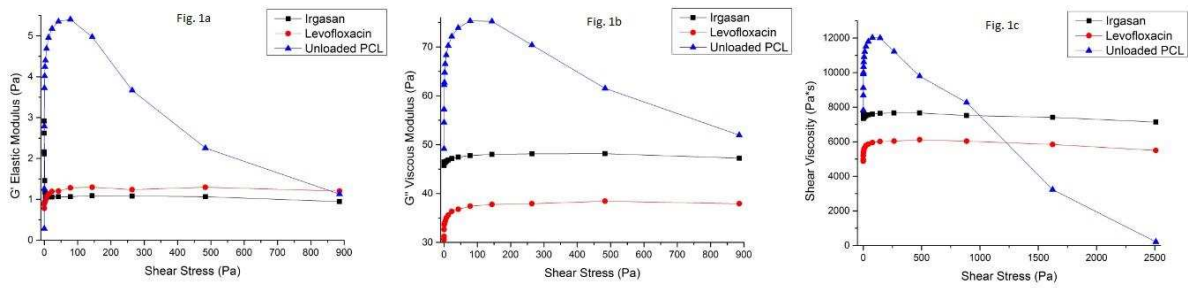
557 **Figure 8a:** The 2D (left) and 3D images show the distribution of $[\text{C}_6\text{H}_9\text{O}_2]^-$ (PCL) in grey
558 and $[\text{C}_{12}\text{H}_6\text{Cl}_3\text{O}_2]^-$ (Irgasan) in yellow. The analysed volume is $100\ \mu\text{m} \times 100\ \mu\text{m}$ on the X-Y

559 axes, and $\sim 3 \mu\text{m}$ on the Z axis: (A) viewed from the top and (B) inclined in order to aid 3D
560 visualization.

561 **Figure 8b:** The 2D (left) and 3D images show the distribution of $[\text{C}_6\text{H}_9\text{O}_2]^-$ (PCL) in grey
562 and of $[\text{C}_{17}\text{H}_{19}\text{FN}_3\text{O}_2]^-$ and $[\text{C}_{18}\text{H}_{19}\text{FN}_3\text{O}_4]^-$ (Levofloxacin) in yellow. The analysed volume is
563 $100 \mu\text{m} \times 100 \mu\text{m}$ on the X-Y axes, and $\sim 3 \mu\text{m}$ on the Z axis: (A) viewed from the top and
564 (B) inclined in order to aid 3D visualization.

565

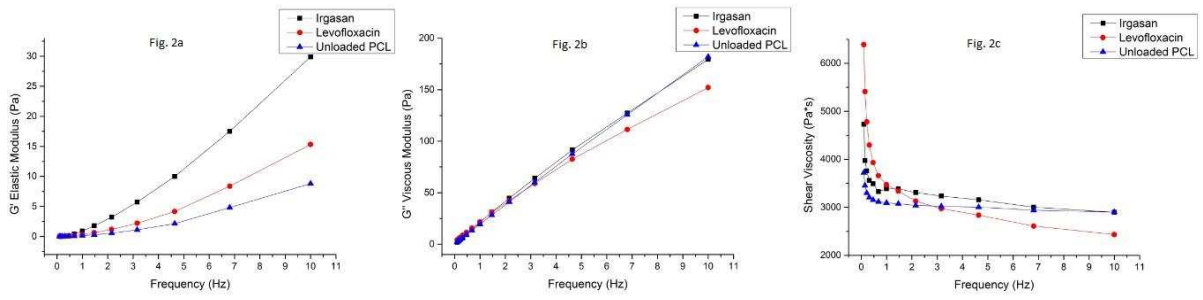
566 **Figure 1a.**



567

568

569 **Figure 2.**

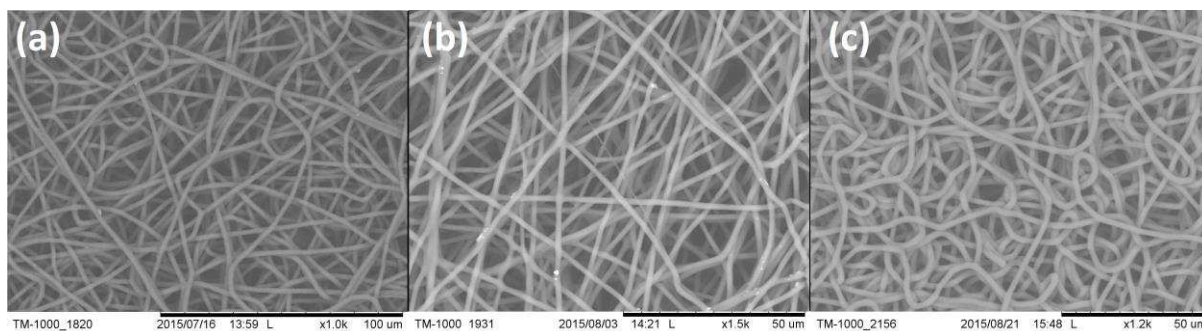


570

571

572

573 **Figure 3.**



574

575

576

577 **Figure 4.**

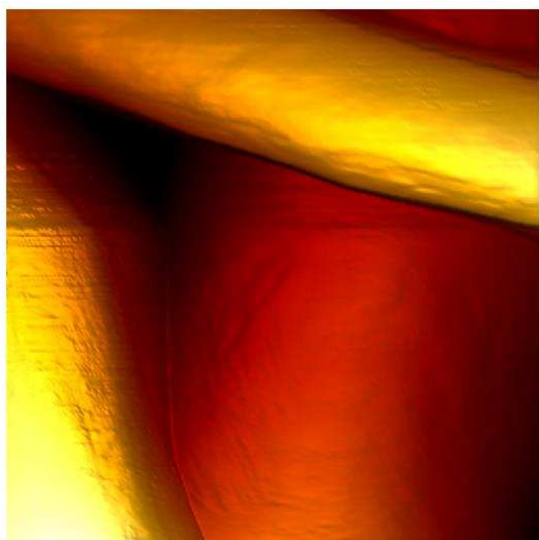


Fig. 4a

400.0 nm

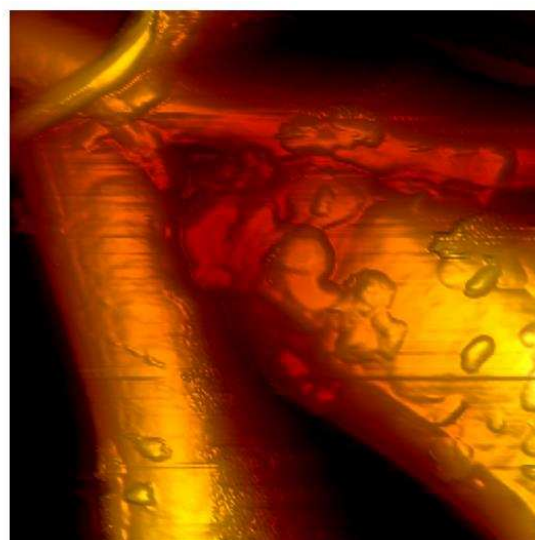


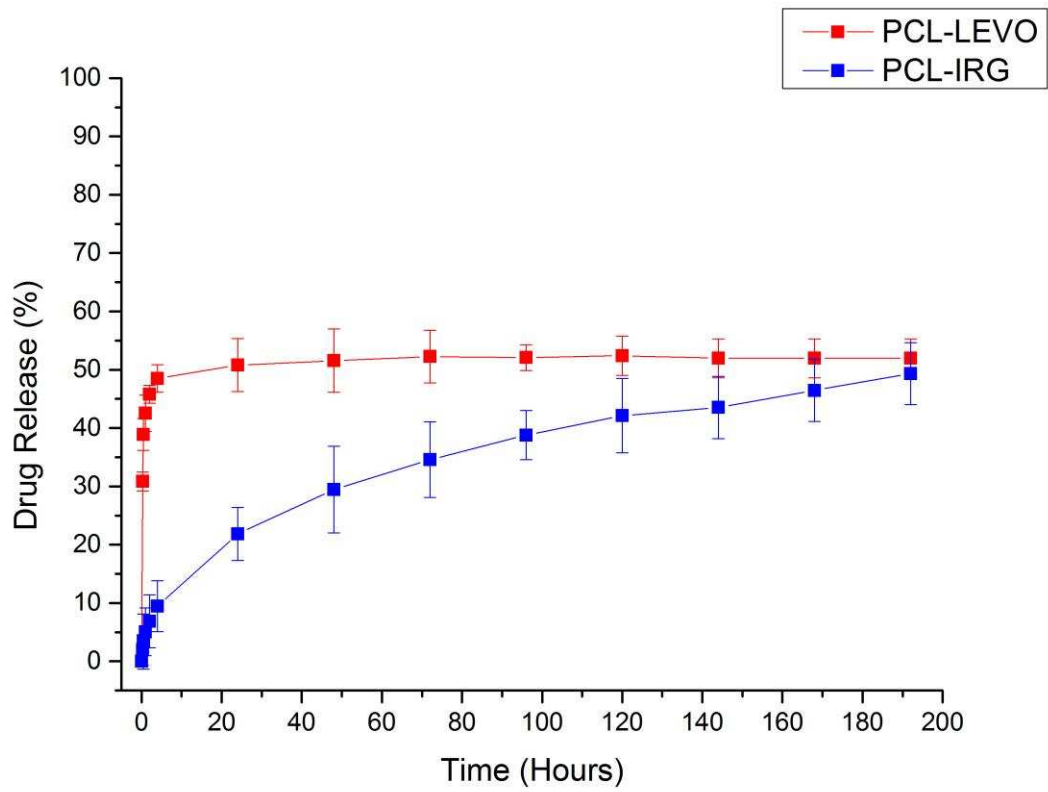
Fig. 4b

1.0 μm

578

579

580 **Figure 5.**



581

582

583

584 **Figure 6.**

585

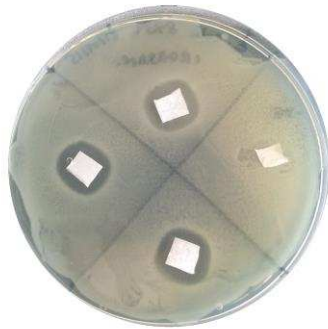
586

587

588

589

590



PCL-Irgasan IZ Average:
E. Coli 8739 0.70±0.50 cm



PCL-Irgasan IZ Average:
S. Aureus 29215 1.80±0.50 cm

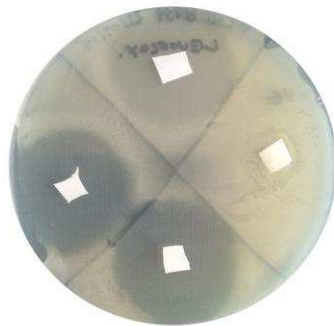
591

592

593

594

595



PCL-Levofloxacin IZ Average:
E. Coli 8739 2.60±0.00 cm



PCL-Levofloxacin IZ Average:
S. Aureus 29215 2.60±0.10 cm

596

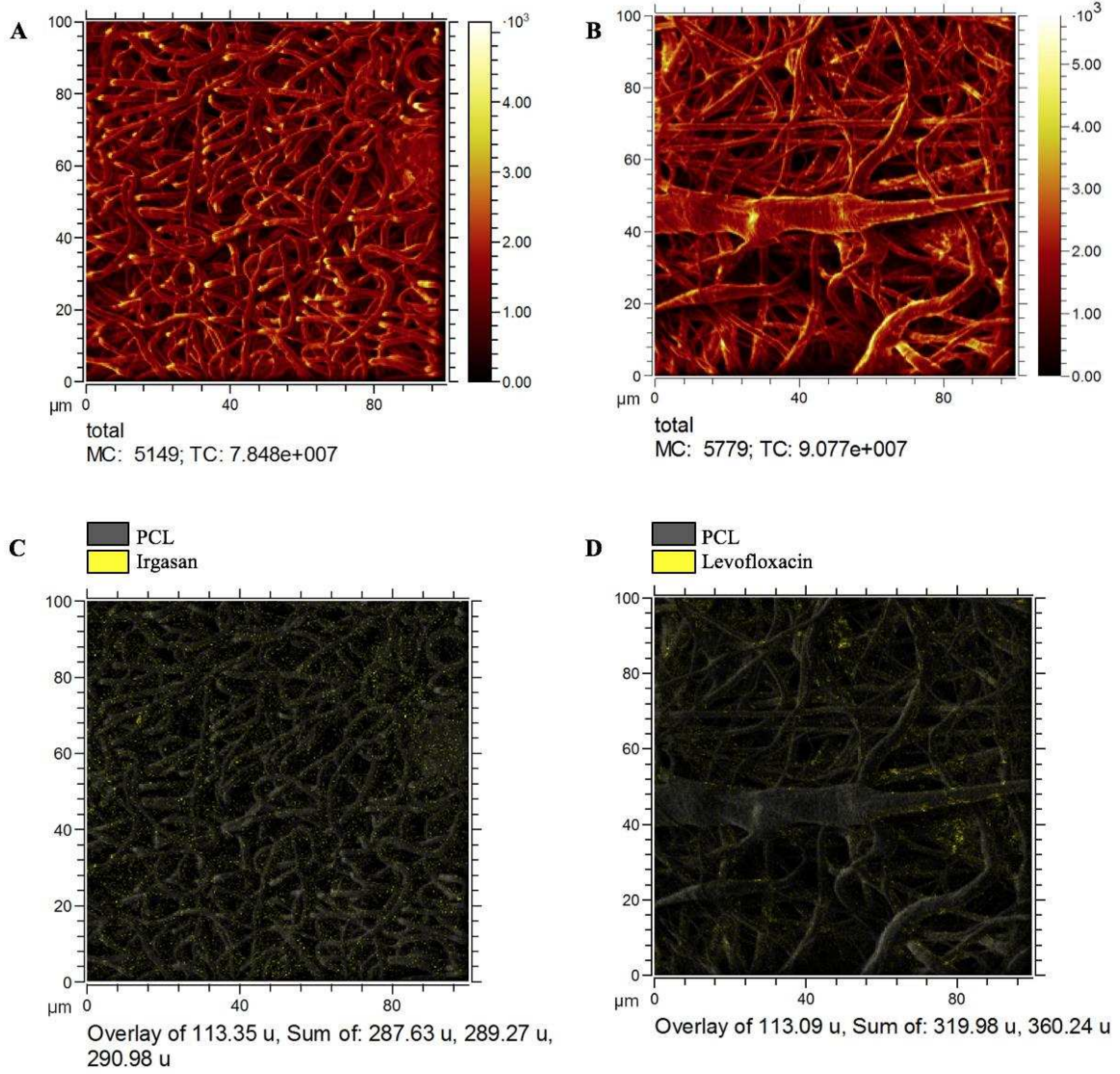
597

598

599

600

601 **Figure 7.**

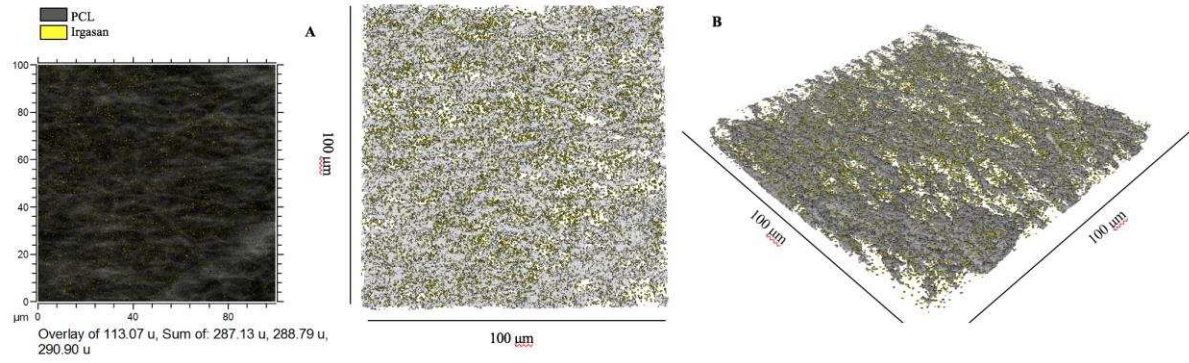


602

603

604

605 **Figure 8a.**



608 **Figure 8b.**

